Ultrasonics 53 (2013) 570–579

Contents lists available at SciVerse ScienceDirect

Ultrasonics

journal homepage: www.elsevier.com/locate/ultras

Modified multi-element synthetic transmit aperture method for ultrasound imaging: A tissue phantom study

Y. Tasinkevych [a,*], Z. Klimonda [a], M. Lewandowski [a], A. Nowicki [a], P.A. Lewin [b]

[a] Institute of Fundamental Technological Research of the Polish Academy of Sciences, Pawinskiego 5B, Warsaw 02-106, Poland
[b] Drexel University, Philadelphia, PA 19104, USA

ARTICLE INFO

Article history:
Received 15 June 2012
Received in revised form 3 October 2012
Accepted 3 October 2012
Available online 17 October 2012

Keywords:
Synthetic aperture imaging
Ultrasound imaging
Directivity function
Beamforming

ABSTRACT

The paper presents the modified multi-element synthetic transmit aperture (MSTA) method for ultrasound imaging. It is based on coherent summation of RF echo signals with apodization weights taking into account the finite size of the transmit subaperture and of the receive element. The work presents extension of the previous study where the modified synthetic transmit aperture (STA) method was considered and verified [1]. In the case of MSTA algorithm the apodization weights were calculated for each imaging point and all combinations of the transmit subaperture and receive element using their angular directivity functions (ADFs). The ADFs were obtained from the exact solution of the corresponding mixed boundary-value problem for periodic baffle system modeling the transducer array. Performance of the developed method was tested using Field II simulated synthetic aperture data of point reflectors for 4 MHz 128-element transducer array with 0.3 mm pitch and 0.02 mm kerf to estimate the visualization depth and lateral resolution. Also experimentally determined data of the tissue-mimicking phantom (Dansk Fantom Service, model 571) obtained using 128 elements, 4 MHz, linear transducer array (model L14-5/38) and Ultrasonix SonixTOUCH Research platform were used for qualitative assessment of imaging contrast improvement. Comparison of the results obtained by the modified and conventional MSTA algorithms indicated 15 dB improvement of the noise reduction in the vicinity of transducer's surface (1 mm depth), and concurrent increase in the visualization depth (86% augment of the scattered amplitude at the depth of 90 mm). However, this increase was achieved at the expense of minor degradation of the lateral resolution of approximately 8% at the depth of 50 mm and 5% at the depth of 90 mm.

1. Introduction

Ultrasound imaging techniques are currently one of the most commonly used modalities for medical imaging in diagnosis and therapeutic procedures. In B-mode (brightness mode) ultrasound typically a linear array of transducers is used to scan the area of interest and the image is obtained using beamforming techniques e.g. delay-and-sum (DAS). To obtain high-quality images the synthetic aperture (SA) algorithms [2–4] have been extensively explored. These algorithms allow the imaging quality obtainable with conventional B-mode imaging (based on line by line data acquisition with transmit focusing) to be improved. This is due to their ability to provide dynamical focusing in both transmit and receive modes. Among several implementations of the SA method that have been reported in literature, the synthetic transmit aperture (STA) approach [5], where all transducer elements are used to receive back-scattered signal at every transmission, has proven to be most suitable for medical ultrasound. In the previous study [1] a modified STA method for ultrasound imaging was developed. The method allowed the contribution of the off-axis targets resulting in broad image clutter especially in the vicinity of the transducer face to be substantially suppressed. Specifically, the simulations, conducted in Matlab® (The MathWorks Inc., Natick MA) using Field II [6,7] software, demonstrated a 12 dB noise reduction, estimated by the lateral cross-sections of point reflectors at the depth of 1 mm, in comparison with conventional STA algorithm. The algorithm was implemented as a weighted sum of the appropriately delayed echo signals with predefined apodization weights calculated for every focal point and transmit-receive combination. The weights were determined using the analytic expression for a far-field radiation pattern of a narrow strip (individual array element) transducer vibrating with uniform pressure amplitude distribution across its surface [8].

The major drawbacks of the STA which restrict its application on clinical scanners are limited penetration depth (since an unfocused wave energy is emitted only by a single element) and a huge amount of data to be processed and computational complexity connected with this. For example, as reported in [1], the processing time for 2D image reconstruction in Matlab® (128 image lines each

* Corresponding author.
E-mail address: yurijtas@ippt.gov.pl (Y. Tasinkevych).

0041-624X/$ - see front matter © 2012 Elsevier B.V. All rights reserved.
http://dx.doi.org/10.1016/j.ultras.2012.10.001

comprised of 512 spatial samples) was about 30 s on PC running Windows 7 x64 with Athlon 64 X2 Dual Core 5600+, core speed 2.8 MHz. The memory requirements for storage of recorded RF echo signals with 5500 samples (sampling frequency f_s = 40 MHz) for 128 emissions was approximately 0.18 GB of RAM (see discussion in Section 3.2).

To resolve the issues of limited penetration depths and computational complexity (to some extent) the multi-element synthetic transmit aperture (MSTA) method described in [9] seems to be suitable. At each time a subaperture comprised of several grouped elements transmits an unfocused ultrasound wave, emulating the radiation pattern of a (virtual) point source, and all the elements receive the echo signals. This allows the emitted energy to be increased (several elements emit simultaneously in MSTA instead of one in STA), which, in turn, leads to increase of the penetration depth. Moreover, a data acquisition cycle can be reduced to several firings. For instance, assuming 8-element non-overlapping transmit subapertures in the case of 128-element transducer array yields 16 emissions in the MSTA method for full data acquisition cycle. This results in eight time higher frame rate in comparison with conventional STA (128 emissions). Moreover, an eight time less memory for recorded RF echoes is required. This makes the MSTA method a likely candidate for clinical applications.

However, when the element size is comparable to the wavelength of the interrogating wave an application of the simple point source model to reconstruct the image leads to errors and artifacts worsening the quality of the overall image in a similar manner as in the case of STA discussed in [1].

The main aim of this work was to develop a modified MSTA method which alleviates these drawbacks. It takes into account the directivity of the transmit subaperture, comprised of several elements, and of the receive element in order to eliminate the influence of the off-axis targets and improve imaging quality. To this end the approach reported in [1] was further developed and generalized for the MSTA method. Namely, a system of predefined apodization weights was introduced for each focal point in the image and all possible combinations of transmit subaperture and receive element. However, in transmit mode the apodization weights were determined using semi-analytic approach for evaluation of the far-field radiation pattern of a periodic baffle system, modeling the transducer array [10], which was considered suitable in this case. The approach presented in [10] allows the interactions between individual elements of the transducer array to be accounted for in the full-wave analysis of the boundary-value problem for periodic baffle array with arbitrary aperiodic excitation.

As shown in this paper the application of proposed apodization weights allowed the quality of the synthesized images to be improved. Specifically, the broad image clutter (hazy blurring artefacts, observable in the case of the conventional MSTA algorithm) resulting from the off-axis reflections were considerably deprecated, particularly in the imaging region near the transducer aperture. This is critical, for example, in breast and skin imaging. Also, the reflections from off-axis targets lead to the image quality degradation especially in bone tissue imaging with conventional medical ultrasound systems [11]. Therefore, the image enhancing techniques are necessary to improve clinical applicability ultrasound imaging of bone tissue. For example, in [12] a minimum variance beamforming was introduced to compensate for the shadowing effects resulting in noisy ultrasound images of tissue in the bone vicinity. In this context the proposed extension of the MSTA method seems to be promising for enhancing of the bone tissue medical imaging as well.

The rest of the paper is organized as follows. In the next section the theoretical background of the MSTA algorithm and its extension are given. Also the main results of the full-wave analysis of the mixed boundary-value problem for periodic baffle array presented in [10] and directly connected with evaluation of the transmit subaperture ADF are referenced here. Next, in Section 3 the performance of the proposed modified MSTA algorithm is tested using synthetic aperture data of point reflectors simulated using Field II for the case of 4 MHz 128-element transducer array with 0.3 mm pitch and 0.02 mm kerf (emulating a linear transducer used in experimental measurements). Simulations were further validated using experimentally obtained synthetic aperture data of the tissue-mimicking phantom (Dansk Fantom Service, model 571) collected using the SonixTOUCH Research system (Ultrasonix Medical Corporation, Richmond, BC, Canada). The scanner was equipped with a linear transducer model L14-5/38: a 128-element transducer with 0.3 mm element pitch, 0.02 mm kerf and 70% fractional bandwidth, excited by two cycles of transducer's center frequency equal 4 MHz. The discussion of the results is provided in Section 4. Finally, in Section 5 the conclusion of this work are summarized.

2. Background theory

In the multi-element synthetic transmit aperture (MSTA) imaging approach a transmit subaperture comprised of several elements is used to emit unfocused wavefront which interrogates the region of interest in the medium as illustrated in Fig. 1.

The back-scattered waves are received by each element independently and the resulting RF echo signals are digitized and stored in memory for further processing. For an N-element array, N_t – element transmit subaperture and N_{sh}-element shift of the transmit subaperture between subsequent emissions, there are $M = \lceil (N - N_t)/N_{sh} \rceil$ emissions in each cycle altogether, where $\lceil x \rceil$ denotes the integer ceiling of x. Assuming $N_t = 1$ results in conventional STA algorithm. In the case of MSTA the frame rate is increased by N/M as compared to the STA method due to decrease of the total number of emissions, which speeds up the data acquisition process. For N-element aperture upon completion of the data acquisition cycle $M \times N$ RF echo signals are recorded for further image synthetisation. Therefore, in comparison with the STA method the MSTA requires also N/M times less memory storage.

The post-processing which includes coherent summation (DAS) of all received RF echoes with dynamical transmit and receive focusing at each imaging point is performed then. For the N-element transducer array at each point in the image, the final focused signal can be expressed as follows:

$$A_{\mathrm{MSTA}}(r,\theta) = \sum_{m=1}^{M}\sum_{n=1}^{N} y_{m,n}\left(\frac{2r}{c} - \tau_{m,n}\right), \tag{1}$$

where $y_{m,n}(t)$ denotes the RF echo signal recorded by nth receive element and corresponding with interrogation pulse emitted by mth transmit subaperture. The round-trip delay $\tau_{m,n}$ is determined by the geometric distance from the imaging point to the transmit subaperture and receive element and is given by expression:

$$\tau_{m,n} = \tau_m + \tau_n, \quad 1 \leqslant n \leqslant N, \quad 1 \leqslant m \leqslant M, \tag{2}$$

where the corresponding transmit (τ_m) and receive (τ_n) delays, relative to the focal point (r, θ), are:

$$\tau_i = \frac{1}{c}\left(r - \sqrt{r^2 + x_i^2 - 2x_i r\sin\theta}\right), \quad i = m, n. \tag{3}$$

In the above equation x_m, x_n are the positions along the x-axis of the mth transmit subaperture and nth receive element, respectively; r and θ are the polar coordinates of the focal point with respect to the origin, placed in the center of the transducer's aperture (see Fig. 1). The first and second summations in Eq. (1) correspond to the transmit and receive dynamical focusing, respectively (transmit and receive delays are dynamically updated for every

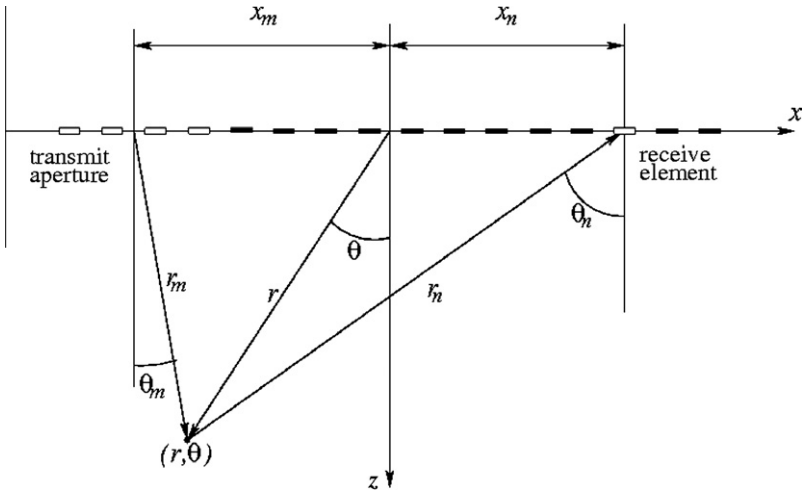

Fig. 1. Spatial diagram illustrating the MSTA beamforming. The round trip delay is determined by the geometric distance between the imaging point and transmit subaperture and receive element centers.

imaging point and every transmit-receive combination). The angular dependence is not taken into account in the point-like source model applied in Eq. (1). However, when the width of the array element is comparable to the wavelength, corresponding to the nominal frequency of the emitted signal, the point-like source model becomes inaccurate, as was reported in the previous study concerning conventional STA method [1]. The reflections from off-axis targets lead to the broad image clutter (hazy blurring artefacts) observable especially in the vicinity of the transducer face. To improve imaging quality in the same way it was done to improve the display obtainable with the STA method [1] the ADFs of the transmit subaperture and receive element need to be accounted for. The ADFs influence the partial contributions of the resulting signal $A_{MSTA}(r, \theta)$ in Eq. (1) depending on the mutual positions of the focal point and transmit-receive pair, determined by the angles θ_m, θ_n (see Fig. 1). They can be incorporated into the MSTA algorithm in a similar manner it was done in the case of the STA method discussed in [1]. Namely, the predefined apodization weights can be introduced into Eq. (1), which yields:

$$A^{\mathrm{mod}}_{\mathrm{MSTA}}(r,\theta) = \sum_{m=1}^{M}\sum_{n=1}^{N} w_{mn} y_{m,n}\left(\frac{2r}{c} - \tau_{m,n}\right), \qquad w_{mn} = f_T(\theta_m) f_R(\theta_n), \quad \theta_i = \theta_i(r,\theta), \quad i = m,n, \tag{4}$$

where $\theta_i(r, \theta)$, $i = m, n$ are the corresponding observation angles for the transmit subaperture and receive element, and $f_T(\theta_m)$, $f_R(\theta_n)$ are their directivity functions, respectively. It is worthwhile to note, that the angles θ_m and θ_n depend on the spatial position of the focal point (r, θ).

In the case of STA algorithm [1] the ADF of single element, used both in transmit and receive modes, was approximated by a far-field radiation pattern of a narrow strip transducer [8]. In the case of MSTA method for evaluation of directivity function of the transmit subaperture, comprised of several (4 up to 16, as evidenced in the Section 4) elements another approach is proposed in this work.

Specifically, the apodization weights can be determined using a semi-analytic approach for evaluation of the ADF of a periodic baffle system, modeling the transducer array [10]. It allows the interactions between individual elements of the transducer to be accounted for in the full-wave analysis of the corresponding boundary-value problem. The solution was obtained in the spatial spectrum domain. Namely, the (spatial) Fourier transform of the pressure field distribution on a baffle plane was used for the far-field radiation pattern evaluation. The nice feature of the method is that the reciprocal influence of the array elements is accounted for in the full-wave analysis of the wave excitation or scattering problems.

In the considered mixed boundary-value problem the normal acoustic vibration vanishes on baffles [13] and between them there are acoustically soft domains where the acoustic pressure vanishes, or is given constant values in the case of the wave excitation problem. The solution was obtained using the BIS-expansion method [14], which was successfully used earlier for solving electrostatic problems in the theory of surface acoustic waves interdigital transducers [15], in the theory of elastic wave scattering by periodic cracks [16], or in generalized form in the theory of electromagnetic wave scattering by periodic gratings [17].

As shown in [10], the ADF of a periodic system of hard acoustic baffles (periodicity along the x-axis direction is assumed, see Fig. 1) can be evaluated from the spatial spectrum (spatial Fourier transform) of the pressure field distribution on the baffle plane as follows:

$$f(\theta) \sim p(k\sin\theta)\cos\theta; \quad k = \frac{\omega}{c} = \frac{2\pi}{\lambda}, \tag{5}$$

where k is the wave-number; c is the sound velocity; ω is the angular temporal frequency. In Eq. (5) p is the spatial spectrum of the pressure distribution on the plane of baffles, which is the solution of the above boundary-value problem and can be written as follows:

$$p(\xi) = p_n(\xi - nK) \equiv p_n(r); \quad \xi = r + nK; \quad n = \lfloor \xi \rfloor, \quad K = 2\pi/\Lambda, \tag{6}$$

where ξ is the spatial spectrum variable in the x-axis direction; $\lceil x \rceil$ is the integer floor of ξ. In Eq. (6) $r \in (0, K)$ is an arbitrary spatial wave-number, constrained to one Brillouin zone, introduced for the sake of uniqueness of the pressure distribution on the plane $z = 0$:

$$p(x) = \sum_n p_n \mathrm{e}^{-j(r+nK)x}, \qquad p_n = \frac{j}{r+nK}\sum_m \alpha_m S_{n-m} P_{n-m}(\cos\Delta); \quad \Delta = \pi(1 - d/\Lambda), \tag{7}$$

where p_n are the Bloch amplitudes; P_n are the Legendre polynomials; d is the baffle width and Λ is the period (transducer pitch); $S_n = 1$ for $n \geqslant 0$ and 0 otherwise. In Eq. (7) α_m are the unknown expansion coefficients (dependent on r) representing the corresponding Bloch

components p_n. The coefficients α_m can be obtained by solving the system of linear equations [5]:

$$\begin{aligned}&\sum_m \alpha_m \left[j\frac{\eta}{\xi} S_{n-m} - 1 \right] P_{n-m}(\cos \Delta) = 0 \\ &\sum_m (-1)^m \alpha_m P_{-r/K-m}(-\cos \Delta) = j\frac{K}{\pi} \tilde{p}_l e^{jrl\Lambda} \sin \pi r/K,\end{aligned} \tag{8}$$

where $\tilde{p}_l = 1, l = 0, \ldots, N_t - 1$, and 0 otherwise are given constant pressures of the corresponding active elements (slots in the considered boundary-value problem formulation) which model the N_t-element transmit subaperture. In Eq. (8) the summation over a finite domain $m \in [-M, M]$ is assumed and $n \in [-M, M]$, or in the other words, there are $2M + 1$ Bloch orders accounted for in the expansion of $p(x)$, Eq. (7). This assumption allows the problem to be reduced to numerical solving of the truncated system of linear equations, Eq. (8), for unknown coefficients α_m. The truncation index M is determined by the BIS-expansion approximation [10], stating that for sufficiently large M (to be defined below) one may assume:

$$\frac{\eta}{\xi} \equiv \frac{\eta}{r + nK} = jS_\xi \tag{9}$$

for any $n > M$ (see Eq. (6) for definition of n). In the above condition η is the spatial spectrum variable in the z-axis direction (harmonic dependence of the pressure field on z is assumed in standard form $e^{-jz\eta}$):

$$\eta = \begin{cases} \sqrt{k^2 - \xi^2}, & |\xi| \leqslant k, \\ -j\sqrt{\xi^2 - k^2}, & |\xi| > k. \end{cases} \tag{10}$$

The value of η in Eq. (9) is chosen so that the solution for radiated pressure field presents outgoing wave, or, alternatively, the scattered field vanishes at $z \to \infty$ in the scattering case. Typically, for $k \sim K$ it is sufficient to take into account only several Bloch components p_n in the solution for the pressure field in Eq. (7). In the numerical examples, shown in the next section, $M = 16$ is applied, which yields the spectral variable ξ in the domain limited by the upper bound $\xi_{\max} \approx 20k$ (for $\Lambda = 0.3$ mm, 4 MHz operating frequency and $c = 15{,}000$ m/s). In this case $\eta/\zeta \approx j0.9987$ resulting in 0.13% rational error in the BIS-expansion approximation, Eq. (9), which accuracy is acceptable for numerical analysis.

In the case of a single-element receive aperture the directivity function and corresponding apodization weights in Eq. (4) can also be evaluated using Eq. (5), if $\tilde{p}_l = \delta_{l0}$ is applied in Eq. (8), where δ - is the Kronecker delta.

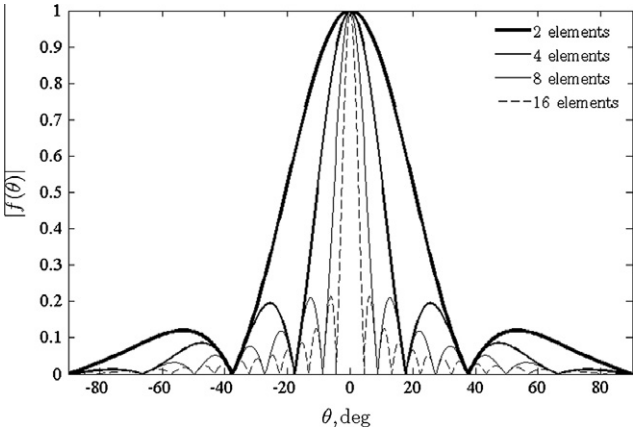

Fig. 2. Angular directivity functions for 2-, 4-, 8- and 16-element subapertures; operating frequency was 4 MHz corresponding to $\Lambda/\delta \approx 0.8$; the element width $d = 0.28$ mm and 0.02 mm kerf was assumed.

Fig. 2 illustrates the computed examples of the ADFs obtained using the above approach for 2-, 4-, 8- and 16-element subapertures and 4 MHz operating frequency, 0.3 mm pitch and $c = 1500$ m/s (the values corresponding to those used in the numerical experiments in the next Section).

The directivity function given by Eq. (5) was used in the modified MSTA algorithm for evaluation of the apodization weights in Eq. (4), both in transmit ($f_t(\theta)$) and receive ($f_r(\theta)$) modes.

3. Methods

To verify the performance of the proposed modified MSTA method it was tested using the data obtained by Field II simulation program for Matlab® and from experimental measurements. The main stress was set on comparison between the images produced using the conventional MSTA, Hamming and Blackman windows enhanced MSTA and the modified STA algorithms.

3.1. Field II simulated point-reflector data

To estimate the lateral resolution and penetration depth obtainable with the modified MSTA method as compared to the conventional MSTA, the Field II simulated synthetic aperture data of point reflectors were used. To this end a linear array transducer with 128 elements and a center frequency of 4 MHz was modeled using *xdc_linear_array* function. The pitch was 0.3 mm and the kerf 0.02 mm which yielded the maximum accessible aperture size of 38 mm for this transducer. These parameters (the center frequency, the pitch and the kerf) were chosen to mimic the Sonix L-14-5/8 array transducer used in experiments (see discussion in the next section). The one sine cycle burst of center frequency equal 4 MHz was assumed as the transducer excitation. The point reflectors were placed in seven columns, each spaced 4.9 mm apart laterally (this corresponds to 16 transducer pitches). The columns were centered with respect to the transducer middle point for convenience. In each column reflectors were spaced 5 mm axially starting from the depth of 1 mm. Such arrangement of point reflectors, covering entire imaging region, was considered to be convenient for visual assessment of the imaging quality in the whole area. It enabled estimation of the spatial resolution at different depths using corresponding lateral cross-sections of 2D images. The temporal sampling rate of 40 MHz was chosen so that the Nyquist criterion was satisfied. The back-scattered RF echo signals with 5500 temporal samples were simulated using a *calc_scat_multi* function of the Field II. To emulate the MSTA mode, during each pulse emission the corresponding transmit subapertures were selected using *ele_apodization* function by setting the values of 1 for active elements and 0 otherwise. To enable accurate quantitative estimates of the lateral resolution 2048 image lines were synthesized (16 image lines per transducer pitch). Every image line had 5000 spatial samples for 100 mm visualization depth corresponding to 50 samples per mm.

3.2. Experimentally obtained tissue-mimicking phantom data

To demonstrate the improvements in image contrast offered by the modified MSTA algorithm the image reconstruction of experimentally obtained synthetic aperture data was performed. An extra large scan- and elevation-plane tissue mimicking phantom model 571 (Dansk Fantom Service [18]) with attenuation of the background material of 0.5 dB/(MHz cm) was used in experiments. The visualized region of the phantom consisted of a collection of cysts with the diameters 2, 4, and 8 mm, being representative of those encountered in clinical practice as suggested in [18]. The cysts were distributed in depth starting from 1 mm, which enabled

comparison of the image contrast obtained with different algorithms. In addition, the cysts placed near the transducer aperture facilitated the demonstration of the noise reduction obtained with the modified MSTA.

The measurements were done using the Sonix-TOUCH Research system (Ultrasonix Medical Corporation, Richmond, BC, Canada). The scanner was equipped with a linear transducer model L14-5/38: a 128-element transducer with 0.3 mm element pitch, 0.02 mm kerf and 70% fractional bandwidth excited by 2 cycles of transducer's center frequency equal 4 MHz.

The RF data collected on each of 128 receive channels were digitized at 12-bit resolution and 40 MHz temporal sampling rate and transferred to a PC for further off-line processing in Matlab® in order to test the developed MSTA image reconstruction algorithm. Every RF echo with 5500 temporal samples was stored in PC RAM. For the conventional STA the total number of samples equal 90e6 required approximately 0.18 GB of RAM. For the MSTA with 4-element non-overlapping transmit subapertures (4-element aperture shift) the total number of temporal samples was reduced to approximately 22.5e6, whereas for 8-element non-overlapping subapertures (8-element shift) the number of samples was further reduced to approximately 11.25e6, which corresponds to 0.045 GB and 0.0225 GB of the RAM, respectively. In the case of 16-element non-overlapping apertures (16-elements shift) and apodization weights applied in receive mode only (see discussion in the Section 4) the corresponding values of 5.6e6 data samples and 0.011 GB of the required RAM were achieved. For experimentally obtained data image reconstruction a total of 128 image lines with 512 spatial samples were synthesized, which yielded for 100 mm visualization depth approximately five samples per mm. The processing time in Matlab® 7.11 on PC running Windows Windows 7 x64 with Athlon 64 X2 Dual Core 5600+, core speed 2.8 MHz was about 8 s for the MSTA using 4-element non-overlapping subapertures (32 emissions), about 4 s for the MSTA using 8-element non-overlapping subaperture (16 emissions) and about 2 s for the MSTA using 16-element non-overlapping subapertures (eight emissions, apodization weights calculated for receive mode). It should be noted that no attempts were made to optimize Matlab code to shorten the image reconstruction time. The issue of processing time reduction can be addressed for example by exploiting a graphics processing unit (GPU) capabilities for SA beamforming (see discussion in Section 6).

4. Results and discussion

4.1. Field II simulations

Examples of 2D visualization of point reflectors are shown in Fig. 3 over a 60 dB dynamic range. Fig. 3a and d show images obtained using the modified MSTA, discussed in this work, and the conventional one, respectively (the case of 4-element transmit subaperture $N_t = 4$ is considered). For comparison, in Fig. 3b and c the images obtained using the MSTA algorithms with Hanning and Blackman apodization weights are shown. The image enhancement, especially in the region adjacent to the transducer's aperture, can be observed. The blurring artefacts clearly visible in Fig. 3b–d in the vicinity of the first row of point reflectors, are substantially (see discussion following Fig. 4) reduced in Fig. 3a processed using the modified MSTA algorithm. Also, the visibility of the point reflectors located at the depth of approximately 80–90 mm is improved (increased penetration depth, see discussion following Fig. 6) in the case of modified MSTA algorithm, see Fig. 3a, when compared with the conventional one, see Fig. 3d.

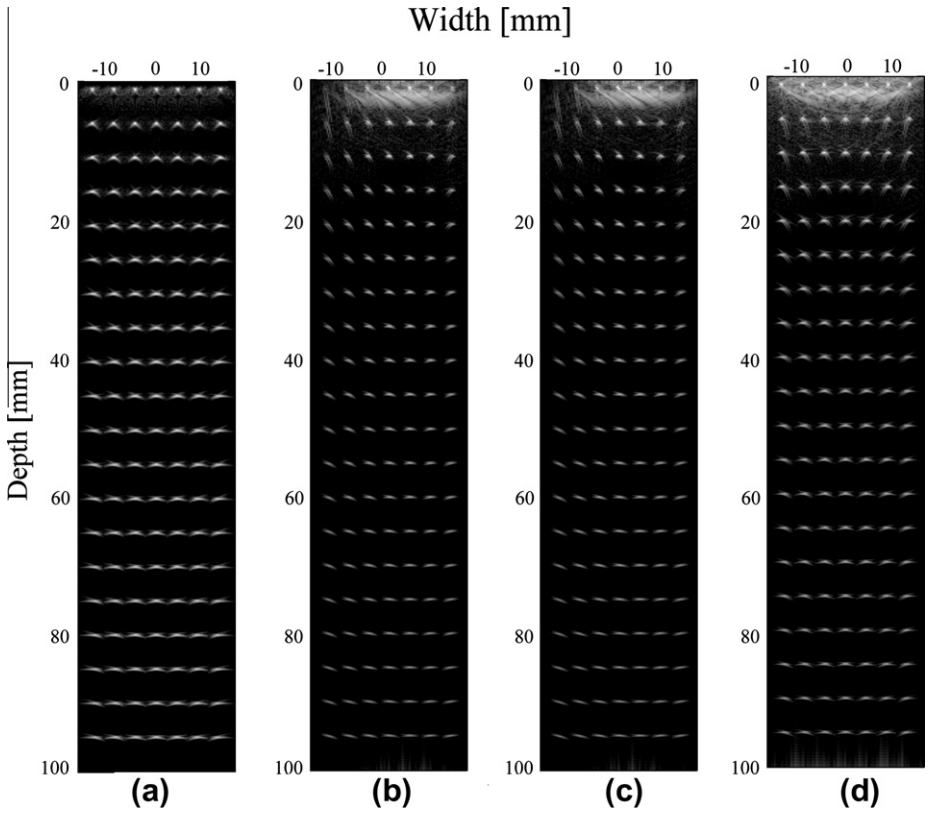

Fig. 3. MSTA image reconstruction of the Field II simulated synthetic aperture data for point reflectors and 4 MHz 128-element transducer array with 0.3 mm pitch and 0.02 mm kerf and $N_t = 4$: (a) modified MSTA algorithm, this work, (b) Hanning apodized MSTA, (c) Blackman, and (d) conventional MSTA. All images are displayed over 60 dB dynamic range.

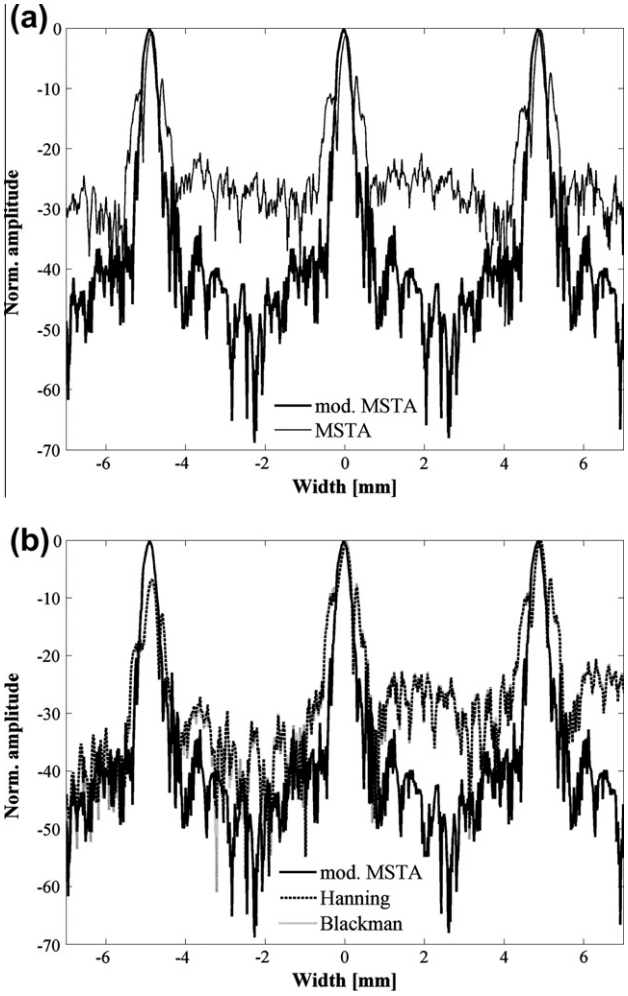

Fig. 4. Lateral cross-section of the first row (depth 1 mm) of point reflectors in logarithmic scale for $N_t = 4$: (a) comparison of the results obtained by the modified MSTA (this work) and conventional MSTA and (b) comparison of the results obtained by the modified MSTA and by the Hanning and Blackman apodized MSTA.

In Fig. 4 the lateral cross-sections of the first row of point reflectors (depth 1 mm) obtained using different methods can be found. The improvement of image quality is also observable in this example. As seen in Fig. 4a, the "noise"-like spatial variations of the scattered signal from the reflectors positioned near the transducer surface are substantially suppressed from approximately −25 dB in the case of MSTA to −40 dB in the case of modified MSTA (measured in midpoints between reflectors). For comparison, the results obtained using the conventional MSTA algorithm with Hanning and Blackman apodization weights are also shown in Fig. 4b. These indicate the "noise" reduction of approximately −27 to 30 dB as compared to the conventional MSTA.

In Fig. 5 the normalized axial cross-section of the central column of point reflectors is shown. The depth up to 4 mm covering the vicinity of the first reflector is visualized for convenience. The "noise" reduction from approximately −14 dB (measured at the depth of 2.5 mm) obtained when applying conventional MSTA algorithm to approximately −23 to 25 dB in the case of Hanning and Blackman apodization weights or −50 dB in the case of modified MSTA algorithm considered in this work, can be observed.

An increase in penetration depth is illustrated in Fig. 6, where a detailed view of the axial cross-sections (central column) showing the maxima of the scattered echo signals as a function of depth are presented. As shown in Fig. 6a and b for $N_t = 4$, the scattered echo amplitude obtained using the modified MSTA algorithm are 1.56

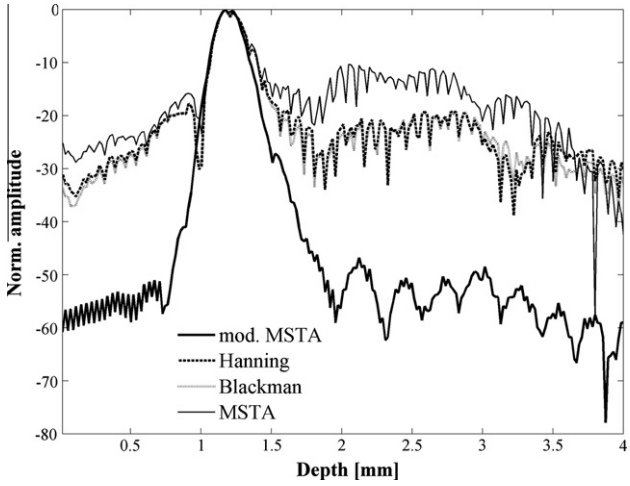

Fig. 5. Normalized axial cross-section of the central column of point reflectors for $N_t = 4$ Thick solid line – modified MSTA, this work, thin solid line – conventional MSTA, dotted line – Hanning apodized MSTA, dashed line – Blackman apodized MSTA.

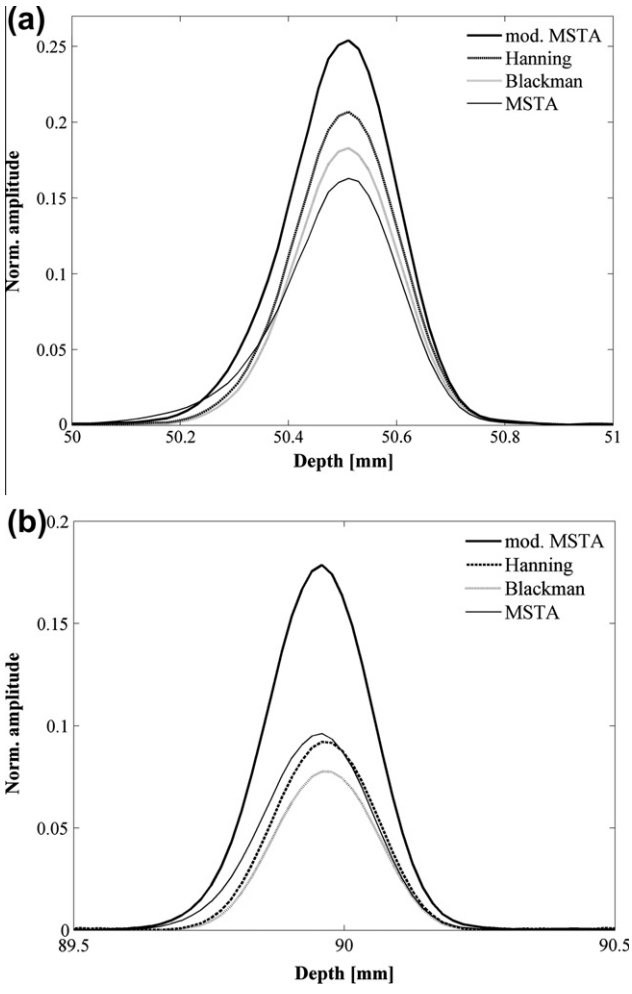

Fig. 6. Normalized axial cross-sections of the image line coinciding with the central column of point reflectors at different depths: (a) 50 mm and (b) 90 mm and $N_t = 4$. Thick solid lines – modified MSTA, this work, thin solid lines – conventional MSTA, dotted lines – Hanning apodized MSTA, dashed lines – Blackman apodized MSTA.

and 1.86 times larger at the depths of 50 and 90 mm as compared to those obtained using conventional MSTA method. A comparison of the results obtained using the modified MSTA algorithm and the

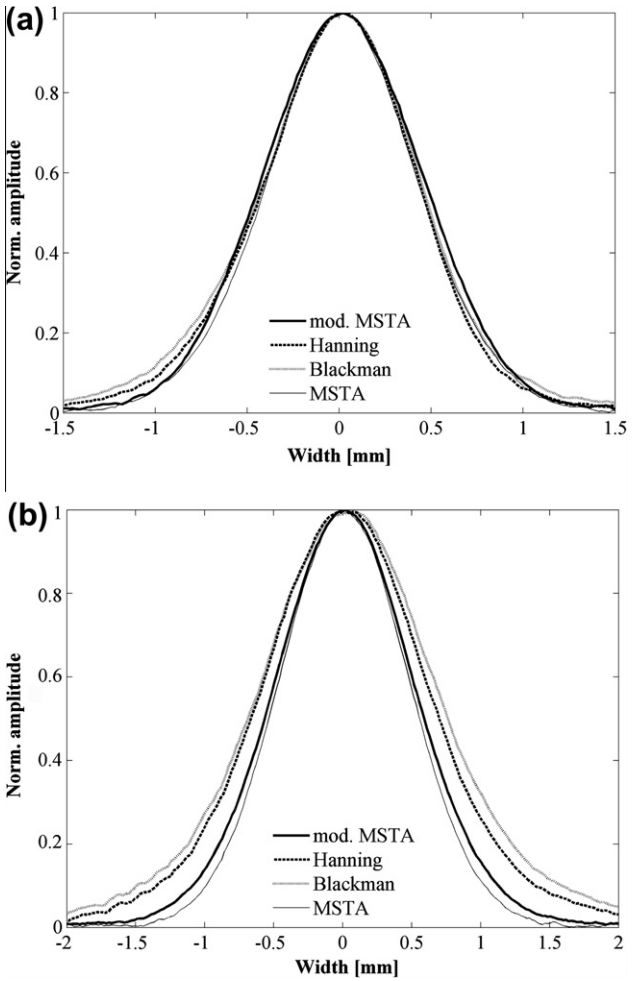

Fig. 7. Normalized lateral cross-section of the scattered signal corresponding to the point reflectors placed in central column at different depths: (a) 50 mm and (b) 90 mm and $N_t = 4$. Thick solid lines – modified MSTA, this work, thin solid lines – conventional MSTA, dotted lines – Hanning apodized MSTA, dashed lines – Blackman apodized MSTA.

conventional MSTA with Hanning and Blackman apodization weights indicate that the scattered amplitudes (at the same depths) are 1.23, 1.94 and 1.39, 2.31 times larger, respectively (see Fig. 6).

Fig. 7 gives an indication of the resolution capabilities of different approaches. There the lateral cross-sections corresponding to scattered echo signal of the point reflectors positioned in the central column at the depths 50 and 90 mm are shown. As illustrated in Fig. 7a and b for the modified MSTA algorithm the lateral resolution is slightly decreased in comparison with the one obtained by using the conventional MSTA. It is quantified here by the full width at half maximum (FWHM). Accordingly, at the axial distance of 50 and 90 mm for the conventional MSTA ($N_t = 4$) the lateral resolution is 0.9316 and 1.0930 mm, respectively. The corresponding data for the modified MSTA are 1.0134 and 1.1565 mm, which represent 8.07% and 5.49% decrease in the lateral resolution at the above identified depths. It is worth noting that the decrease in the lateral resolution diminishes with depth. In the case of MSTA algorithm with Hanning and Blackman apodization weights (dashed and dotted lines in Fig. 7a and b) the respective lateral resolutions are equal to 0.9476 and 1.3634 mm (Hanning) and 0.9691 and 1.3448 mm (Blackman). This corresponds to the respective decreases in lateral resolution of 1.69% and 19.83% (Hanning) and 3.87% and 24.53% (Blackman) as compared to the conventional MSTA processing (it worth to note the increase with depth in the lateral resolution degradation in this case). These data indicate that the modified MSTA algorithm at the depths below 50–60 mm exhibits somewhat lower lateral resolution in comparison with that achieved with Hamming and Blackman apodizations. On the other hand, at the axial distances exceeding 70 mm, the lateral resolution of the modified MSTA algorithm exceeds those that were obtained using Hamming and Blackman windows.

5. Experimental results

Experimental validation of the improvements in image contrast offered by the modified MSTA algorithm are demonstrated in Fig. 8 where the examples of 2D image reconstruction of the experimentally obtained tissue-mimicking phantom (Dansk Fantom Service, model 571 [18]) data are illustrated.

The image enhancement in the vicinity of the array's aperture is clearly observable from comparison of the images shown in Figs. 8a (modified MSTA, this work) and Fig. 8d (conventional MSTA). Similarly, the comparison of the images obtained by the MSTA method with Hanning (Fig. 8b) and Blackman (Fig. 8c) windows with the image of Fig. 8a indicates the improved display structure close to the array's surface. Also, the results shown in Fig. 8, demonstrate that the image contrast of the cysts located at the axial distance exceeding 40 mm is also slightly improved (visual assessment).

The modified MSTA method discussed in this work performs well if the number of elements in transmit subaperture is not greater than approximately 14–16. For larger number of elements the increasing directivity of the transmit subaperture leads to the 'transmit beam separation' phenomenon (see example in Fig. 9b) provided that non-overlapping transmit subapertures are considered. For example (see Fig. 9), for 16-element subaperture and the 4 MHz 128-element transducer array with 0.3 mm pitch and 0.02 mm kerf the ADF's angular width measured at the reference level of −6 dB is approximately 5° (see Fig. 2). This corresponds to approximately 4.3 mm spatial beam-width at the depth of 50 mm ($w \approx \alpha R$, w being the spatial width at the depth R; α – is the angular width). The above estimated value of the beam-width is comparable with the transmit subaperture size, being equal approximately 4.9 mm. This influence of the transmitted beams separation is illustrated in Fig. 9 where the examples of image reconstruction of the same tissue-mimicking phantom (see Fig. 8) are shown for the case of conventional MSTA (Fig. 9a) and modified MSTA (Fig. 9b) using 16-element non-overlapping transmit subapertures (the aperture shift $N_{sh} = 16$ is assumed). The deterioration of the synthesized images can be eliminated provided the smaller subaperture shift is used. For example, applying $N_{sh} = 8$ or $N_{sh} = 4$, as illustrated in Fig. 9c and d, the transmitted beams separation effect can be suppressed. However, it should be noted, that the decrease of N_{sh} from 16 to 4 leads to four times longer image reconstruction time due to the four times increase in the number of recorded RF echoes (32 emissions instead of 8). This limitation can be alleviated to some extent by using the MSTA algorithm with larger subaperture shifts ($N_{sh} = 8$, up to 16 for 16-element transmit subaperture) but with the corresponding apodization weights applied in the receive mode only [19]. This is illustrated in Fig. 10, where the same tissue-mimicking phantom data were reconstructed using the modified MSTA method with $N_t = 16$ and different N_{sh} assumed. The apodization weights were evaluated in Eq. (4) only in receive mode ($f_T(\theta) \equiv 1$ was applied).

As shown in Fig. 10a, application of the apodization weights only in receive mode provides better image quality (by visual assessment) of the cysts located in the vicinity of the transducer aperture in comparison with conventional MSTA (Fig. 9a). It also allows the transmitted beam separation phenomenon to be suppressed to some extent in comparison with modified MSTA having apodization weights applied both in transmit and receive modes (Fig. 9b).

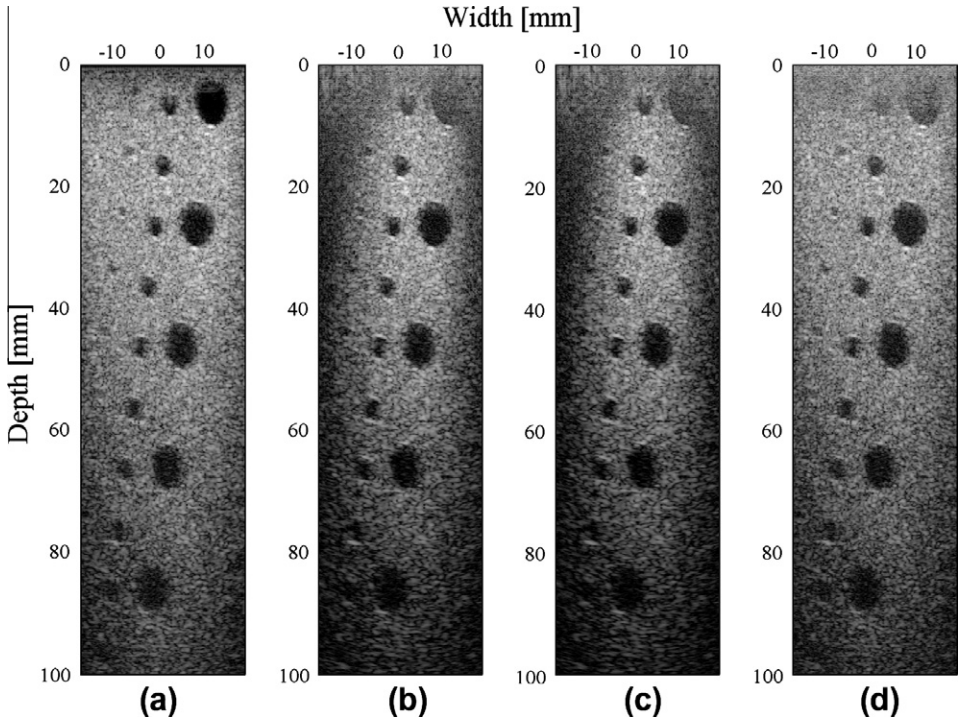

Fig. 8. MSTA image reconstruction of the measurement synthetic aperture data for tissue-mimicking phantom (Dansk Fantom Service, model 571 [18]) and 4 MHz 128-element transducer array with 0.3 mm pitch and 0.02 mm kerf, $N_t = 4$: (a) modified MSTA, this work and (b) Hanning apodized MSTA, (c) Blackman apodized MSTA, and (d) conventional MSTA. All images are displayed over 50 dB dynamic range.

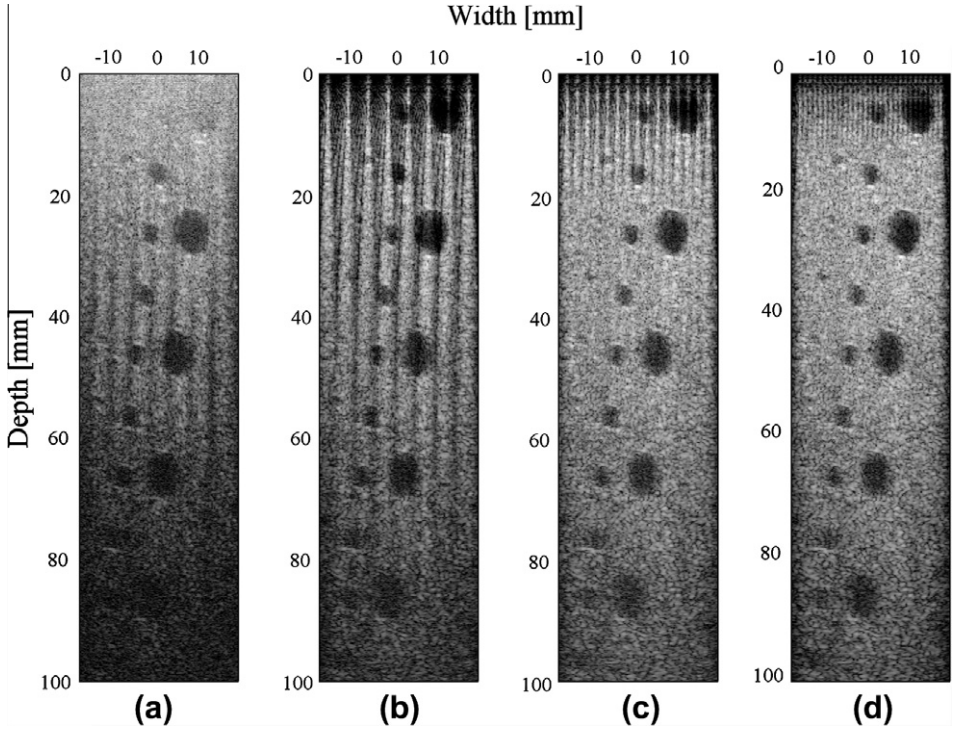

Fig. 9. MSTA image reconstruction of the measurement synthetic aperture data for the same phantom and transducer array; $N_t = 16$: (a) conventional MSTA, $N_{sh} = 16$, (b) modified MSTA, this work, $N_{sh} = 16$, (c) modified MSTA, $N_{sh} = 8$, and (d) modified MSTA, $N_{sh} = 4$. All images are displayed over 50 dB dynamic range.

6. Conclusions

In this work the modified multi-element synthetic transmit aperture (MSTA) algorithm for ultrasound imaging was presented and discussed. In analogy to the STA method, discussed in [1] the algorithm was realized as a weighted sum of properly delayed RF echoes. The corresponding weights were evaluated using angular directivity functions of the corresponding transmit and receive subapertures for each focal point in the image. For efficient computation of the far-field radiation patterns the results of the previous

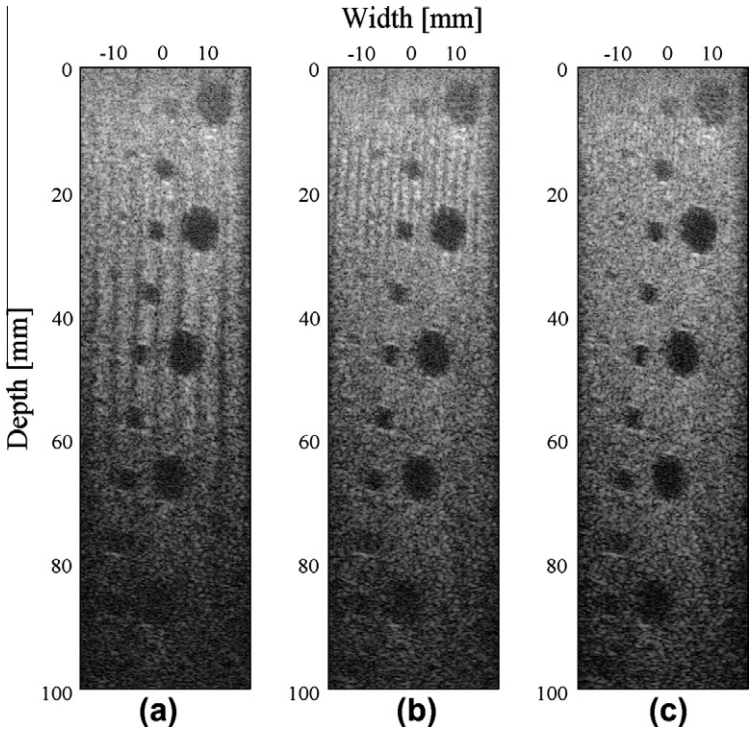

Fig. 10. Image reconstruction of the measurement synthetic aperture data for the same tissue-mimicking phantom and transducer array using modified MSTA method with $N_t = 16$ and apodization weights applied only in receive mode: (a) $N_{sh} = 16$, (b) $N_{sh} = 8$ and (c) $N_{sh} = 4$. All images are displayed over 50 dB dynamic range.

study concerning the analysis of generation and scattering of the acoustic waves by periodic baffle system were used [10]. The predicted improvements in the image quality and the penetration depth were verified using experimentally obtained synthetic aperture data of tissue-mimicking phantom and Field II [6,7] simulated synthetic aperture data of point reflectors. It was shown, that using the modified MSTA algorithm considerable improvement in the image quality in the immediate vicinity of the transducer surface can be achieved. Specifically, the hazy blurring artefacts observable in the images obtained using the conventional synthetic aperture algorithm were substantially (∼15 dB, see Fig. 5a) suppressed due to the directivity weights applied in the developed algorithm. In addition, an increase in the penetration depth was demonstrated. More specifically, the scattered amplitude increased by the factor of 1.56, 1.86 in the case of the modified MSTA algorithm with $N_t = 4$ in comparison to the conventional one, at the depths of 50 and 90 mm. Concurrently, however, a slight degradation of the lateral resolution was observed; namely, at the depths of 50, 90 mm the modified MSTA algorithm provided the lateral resolution which was 8.07% and 5.49% worse, respectively, than that achieved with the conventional MSTA method. On the other hand this decrease in the lateral resolution diminishes with increasing penetration depth.

The numerical results of tissue-mimicking phantom visualization using experimentally obtained data showed improvement of the image contrast in the phantom region in the vicinity of the transducer surface. Also, deeper located cysts (axial distance larger than 40 mm) were visualized with slightly improved contrast too.

It was demonstrated that the proposed algorithm is capable of improving the display quality provided the transmit subaperture is comprised of no more than approximately 16 elements. This is due to the transmitted beam separation which is related to decreasing angular beam-width. It was demonstrated, however, that this phenomenon can be eliminated if the proposed apodization weights are applied in receive mode only, which still yields improved imaging quality as compared to the conventional MSTA algorithm.

It should be noted that the signal processing involved allowed off-line image reconstruction, only, similarly as in the case of STA method [1]. To the best of the authors' knowledge the STA imaging is currently realized in research ultrasound imaging systems only and no commercial medical system is available for clinical application. However, the MSTA method discussed in this work offers better frame rate as compared to the STA. For instance, using 128-element array transducer with 8-element transmit subaperture and 8-element shift between subsequent emissions the MSTA provides eight times higher frame rate than that obtainable with STA. Moreover, the MSTA requires less computations in comparison with the STA algorithm, which makes it competitive for real-time processing. The most promising approach for reduction of the processing time is acceleration of SA beamforming by using graphics processing unit (GPU) to perform all data processing such as apodization, DAS and other related tasks [20]. For example, recently the MSTA image reconstruction algorithm was implemented on the research platform utilizing GPU beamformer by Yiu et al. [21]. Their results proved feasibility of real-time SA imaging: for 32 receive channels at 40 MHz temporal sampling and 15 cm visualization depth the 512×255 pixel images were reconstructed at 3000 fps frame rate.

Provided the real-time processing is implemented in commercial scanners, the modified MSTA method would be well suited to be employed in clinical examinations, especially in the applications where the quality of the image in the immediate vicinity of the scanhead is of critical importance such as for instance in skin- and breast-examinations. It also can be used for enhancing of bone tissue medical imaging by eliminating unwanted reflections from the off-axis targets which degrade the quality of the resulting images.

Acknowledgment

Project POIG.01.03.01-14-012/08-00 co-financed by the European Regional Development Fund under the Innovative Economy Operational Programme. Project is governed by Ministry of Science and Higher Education, Poland.

References

[1] Y. Tasinkevych, I. Trots, A. Nowicki, P.A. Lewin, Modified synthetic transmit aperture algorithm for ultrasound imaging, Ultrasonics 52 (2) (2012) 333–342.
[2] J.A. Jensen, S.I. Nikolov, K.L. Gammelmark, M.H. Pedersen, Synthetic aperture ultrasound imaging, Ultrasonics 44 (2006) e5–e15.
[3] S.I. Nikolov, J.A. Jensen, B.G. Tomov, Fast parametric beamformer for synthetic aperture imaging, IEEE Trans. Ultrason., Ferro Elect., Freq. Cont. 55 (8) (2008) 1755–1767.
[4] I.K. Holfort, A. Austeng, J.F. Synnevg, S. Holm, F. Gran, J.A. Jensen, Adaptive receive and transmit apodization for synthetic aperture ultra-sound imaging, Proc. 2009 IEEE Ultrason. Symp. (2009) 1–4.
[5] V. Behar, D. Adam, Optimization of sparse synthetic transmit aperture imaging with coded excitation and frequency division, Ultrasonics 43 (10) (2005) 777–778.
[6] J.A. Jensen, N.B. Svendsen, Calculation of pressure fields from arbitrarily shaped, apodized, and excited ultrasound transducers, IEEE Trans. Ultrason., Ferro elect., Freq. Cont. 39 (2) (1992) 262–267.
[7] J.A. Jensen, Field: a program for simulating ultrasound systems, in: Proc. 10th Nordic-Baltic Conference on Biomedical Imaging published in Medical & Biological Engineering & Computing, vol. 34, No. 1, 1996, pp. 351–353.
[8] A.R. Selfridge, G.S. Kino, B.T. Khuriyakub, A theory for the radiation pattern of a narrow-strip acoustic transducer, Appl. Phys. Lett. 37 (1) (1980) 35–36.
[9] K.L. Gammelmark, J.A. Jensen, Multi-element synthetic transmit aperture imaging using temporal encoding, IEEE Trans. Med. Imag. 22 (4) (2003) 552–563.
[10] Y. Tasinkevych, E.J. Danicki, Wave generation and scattering by periodic baffle system in application to beam-forming analysis, Wave Motion 48 (2) (2011) 130–145.
[11] F.W. Mauldin, K. Owen, M. Tiouririne, J.A. Hossack, The effects of transducer geometry on artifacts common to diagnostic bone imaging with conventional medical ultrasound, IEEE Trans. Ultrason., Ferroelect., Freq. Cont. 59 (6) (2012) 1101–1114.
[12] S. Mehdizadeh, A. Austeng, T.F. Johansen, S. Holm, Minimum variance beamforming applied to ultrasound imaging with a partially shaded aperture, IEEE Trans. Ultrason., Ferroelect., Freq. Cont. 59 (4) (2012) 683–693.
[13] B. Erbas, Scattering of sound waves by an infinite grating composed of rigid plates, Wave Motion 44 (2007) 282–303.
[14] K. Bløtekjær, K.A. Ingebrigtsen, H.A. Skeie, A method for analyzing waves in structures consisting of metal strips on dispersive media, IEEE Trans. Electron. Device 20 (1973) 1133–1138.
[15] E.J. Danicki, Y. Tasinkevych, Nonstandard electrostatic problem for strips, J. Electrostat. 64 (6) (2006) 386–391.
[16] E.J. Danicki, Scattering by periodic cracks and theory of comb transducers, Wave Motion 35 (2002) 355–370.
[17] Y. Tasinkevych, Electromagnetic scattering by periodic grating of PEC bars, J Electromagn. Waves Appl. 25 (5–6) (2011) 641–650.
[18] http://fantom.dk/571.htm.
[19] I. Trots, A. Nowicki, M. Lewandowski, Y. Tasinkevych, Multi-element synthetic transmit aperture in medical ultrasound imaging, Arch. Acoust. 35 (4) (2010) 687–699.
[20] C.J. Martín-Arguedas, D. Romero-Laorden, O. Martínez-Graullera, M. Pérez-López, L. Gómez-Ullate, An ultrasonic imaging system based on a new SAFT approach and a GPU beamformer, IEEE Trans. Ultrason., Ferro elect., Freq. Cont. 59 (7) (2012) 1402–1412.
[21] B.Y.S. Yiu, I.K.H. Tsang, A.C.H. Yu, GPU-based beamformer: Fast realization of plane wave compounding and synthetic aperture imaging, IEEE Trans. Ultrason., Ferro elect., Freq. Cont. 58 (8) (2011) 1698–1705.